STM JOURNALS

Journal of
Refrigeration, Air Conditioning, Heating and Ventilation

ISSN: 2394-1952
Volume 12, Issue 1, 2025
January–April
DOI (Journal): 10.37591/JoRACHV

https://journals.stmjournals.com/jorachv

Research JoRACHV

Improving Indoor Room Air Conditioning Using PID Control

Carlos Armenta-Déu[1,*], Julián Arenas[2]

Abstract

Energy use in building air conditioning contributes significantly to power demand; therefore, in this work, we propose an improved methodology to achieve comfort conditions through PID control assistance. The project develops a mathematical model based on analytical heat transfer equations for comfort conditions by fulfilling the Fanger equation, considering environmental parameters (ambient temperature), metabolic rate, and people's physical activity (internal heat generation) to reduce power consumption and improve energy efficiency. The prediction of building thermal behavior is based on a control system assisted by the PID technique applied to an aerothermal unit that powers the building heating system. We use three methods for heating the building: radiation, forced convection, and radiation-forced convection hybrid method. The combined one provides the best results with higher efficiency among the three methods, reducing the energy use due to a lower heating curve (lower heating power), improving efficiency, and requiring less power from the energy source. Besides, it reduces the heating time to reach the setup temperature inside the building. Theoretical predictions of building temperature match experimental tests run in an inhabited house with accuracy higher than 99%.

Keywords: PID control, mathematical model, building air conditioning, energy efficiency, comfort improvement

INTRODUCTION

Power for heating, ventilating, and air conditioning represents a significant percentage of household energy consumption, requiring increasing power demand from the grid as the population rises and standard comfort conditions improve [1–6].

The energy consumption depends on the setup comfort conditions, equipment type and efficiency, and human habits. Because the comfort, standard conditions are variable depending on climatic region, meteorological conditions, and people's thermal sensation [7–11], it is complex to establish a unique protocol to define how to air condition a room or a building.

Many treaties and scientific research have been developed to study and analyze the heating, ventilation, and air conditioning (HVAC) processes to reach comfortable temperatures in buildings, defining specific methods for air conditioning buildings [12–17].

People use private protocols for room heating and air conditioning, but most of the time, far away from efficient patterns due to ignorance or personal feelings about the right way of setting up temperature control. The principal consequence is inefficient energy use and higher heat losses, resulting in poor thermal performance of HVAC

*Author for Correspondence
Carlos Armenta-Déu
E-mail: cardeu@fis.ucm.es

Professor, Facultad de Ciencias Físicas. Universidad Complutense, Madrid, Spain

Received Date: November 20, 2024
Accepted Date: January 09, 2025
Published Date: January 20, 2025

Citation: Carlos Armenta-Déu, Julián Arenas. Improving Indoor Room Air Conditioning Using PID Control. Journal of Refrigeration, Air Conditioning, Heating and Ventilation. 2025; 12(1): 1–21p.

systems. Because of the poor or none knowledge about the efficient use of heating and refrigeration systems, buildings require an automated protocol to manage the air conditioning process to reach comfort conditions most efficiently.

In this work, we propose an automatic control process based on the PID technique and assisted by Artificial Intelligence to efficiently manage building heating or refrigeration, adapting to variable thermal conditions and human habits.

THEORETICAL BASIS

According to the country climatic zone, the energy requirements for building air conditioning change. In the OEDC countries, around 30% of the energy consumption is devoted for building air conditioning, raising to 50% outside the OECD zone, and to 70% for non-developed countries [18–22].

The ASHRAE standard defines the thermal comfort as a satisfactory mental condition with thermal environment [23]. The thermal comfort conditions are expressed through mathematical relations, relating room temperature and people thermal sensation [24]. The most commonly used are the Fanger equation [25] and the Humphreys thermal neutrality condition [26].

Fanger Thermal Equation

Macpherson identified six parameters influencing thermal comfort: air temperature and speed, relative humidity, mean radiant temperature (MRT), metabolic rate, and clothing level [27]. Other parameters in the comfort analysis relate to the thermal variables, depending on each other or the above parameters.

The Fanger equation establishes the relation between climatic conditions, clothing level, and physical human activity. This equation represents the human body's thermal balance regarding heat exchange with the environment regarding the six principal parameters mentioned before.

Mathematically, the Fanger equation is as follows:

$$\begin{aligned}&(M/A_{DU})(1-\eta)-0.35\left[43-0.61(M/A_{DU})(1-\eta)-P_a\right]-\\&-0.42\left[(M/A_{DU})(1-\eta)-50\right]-0.0023(M/A_{DU})(44-P_a)-\\&-0.0014(M/A_{DU})(34-T_a)=\\&=3.4x10^{-8}\,f_{cl}\left[(T_{cl}+273)^4-(T_{MRT}+273)^4\right]+f_{cl}h_c(T_{cl}-T_a)\end{aligned} \tag{1}$$

The terms involved in Eq. (1) are:
M: Metabolic level,
P_a: Ambient pressure (kPa),
h_c: Convection coefficient,
T_{cl}: Body temperature with clothing (ºC),
f_{cl}: Clothing factor,
T_a: Room temperature (ºC),
A_{DU}: Wet body surface (m^2),
T_{MRT}: Mean radiant temperature (ºC), and
η: Metabolic to thermal energy conversion efficiency.

We can determine the convection coefficient from the expression:

$$\begin{aligned}&h_c=2.05(T_{cl}-T_a)^{0.25} \quad for \quad 2.05(T_{cl}-T_a)^{0.25}>10.4\sqrt{v}\\&h_c=\sqrt{v} \quad for \quad 2.05(T_{cl}-T_a)^{0.25}<10.4\sqrt{v}\end{aligned} \tag{2}$$

v is the wind speed.

On the other hand:

$$T_s = 35.7 - 0.032\left(H/A_{DU}\right) \tag{3}$$

$$\xi_{SW} = 0.42A_{DU}\left[\left(H/A_{DU}\right) - 50\right] \tag{4}$$

With:
T_s: Basal temperature (ºC),
H: Internal heat generation (J), and
ξ_{SW}: Sweating heat losses (J).

Eqs. (1)–(3) show that human thermal comfort depends on clothing type (T_{cl}, f_{cl}), human activity (η, M, A_{DU}), and environmental parameters (T_a, T_{MRT}, P_a).

The thermal comfort equation only applies to people in thermal equilibrium with their surroundings; therefore, we cannot apply it to people's thermal sensations in arbitrary climatic conditions where comfort parameters do not fulfill the Fanger equation. In case we operate out of the thermal equilibrium, the following equation applies:

$$\begin{aligned} PMV = &\left(0.352e^{-0.042\left(M/A_{DU}\right)} + 0.032\right)\left(M/A_{DU}\right)\left(1-\eta\right) - \\ &-0.35\left[43 - 0.61\left(M/A_{DU}\right)\left(1-\eta\right) - P_a\right] - \\ &-0.42\left[\left(M/A_{DU}\right)\left(1-\eta\right) - 50\right] - 0.0023\left(M/A_{DU}\right)\left(44 - P_a\right) - \\ &-0.0014\left(M/A_{DU}\right)\left(34 - T_a\right) - 3.4x10^{-8} f_{cl}h_c\left(T_{cl} - T_a\right) \end{aligned} \tag{5}$$

PMV is the predicted mean vote, which expresses the average value of people's thermal sensation.

We should fulfill Eq. (1) to reach thermal comfort; unfortunately, all parameters involved are variable, which makes the comfort conditions calculation complex; therefore, we have to constrain the variable to current operational ranges, restraining the combination chances; conventional ranges for setup parameters are [28]:

- *Clothing factor:* $f_{cl} \in \{0.0;4\}$, where 0.0 corresponds to nudity and 4 to heavy clothing; current values adopted for f_{cl} are 0.0, 0.6, 0.9, 2.4, and 4.
- *Metabolic Level:* $M \in \{1;5\}$, with three adopted values: 1 for moderate activity, 3 for intermediate, and 5 for intense.
- *Room wind speed:* $v \in \{0.1;10\}$, with current operational values of 0.1, 0.5, 2.0, 5.0, and 10.

Specific sensors register the ambient pressure and temperature inside the room. The convection coefficient is determined from Eq. (2), provided the body surface temperature is considered constant at the standard average value of 37.0ºC [29, 30].

The wet body surface directly relates to human activity, and can be calculated from the expression:

$$A_{DU} = f_A A_{DU} \tag{6}$$

Where the coefficient f_A adopts the following values:

- f_A=0.0 for light or null activity,
- f_A=0.5 for moderate activity, and
- f_A=1.0 for intense activity.

The skin surface of the human body depends on the body weight, height, and gender, male or female. A professional application provides a calculation tool [30] based on existing studies [31–35].

The Mean Radiant Temperature calculation responds to the following expression [36–38]:

$$T_{MRT} = \left[\frac{\left(T_g + 459.67\right)^4 + \left(4.74x10^7 v^{0.6}\right)}{\varepsilon D^{0.4}\left(T_g - T_a\right)} \right]^{1/4} - 459.67 \tag{7}$$

T_g, D, and ε are the black globe temperature, diameter, and emissivity. The black globe is at the room's geometric center.

On the other hand, the metabolic to thermal energy conversion depends on chemical reactions subjected to thermodynamic laws [39–42]; although every person is different, we can accept a 25% efficiency, on average [43].

Table 1 summarizes the status of thermal comfort evaluation regarding the dependent parameters.

The comfort state is closely linked with ambient temperature through a linear relation. Humphrey and Auliciemes propose two options for the linear dependence [44, 45]:

$$\begin{aligned} T_n &= 11.9 + 0.534 < T_a > \quad \textit{Humphrey} \\ T_n &= 17.6 + 0.314 < T_a > \quad \textit{Auliciemes} \end{aligned} \tag{8}$$

The expression proposed by Humphrey overestimates the temperature in summer, while the one suggested by Auliciemes does in winter.

An advanced expression due to Szokolay combines thermal neutrality and stress, yielding [46]:

$$T_n = 17.6 + 0.31 < T_a > \tag{9}$$

Valid for $18.5 < T_n < 28.5$ and relative humidity below 90%.

Bioclimatic Charts

Combining all variables in the previous analysis, we may draw a chart, establishing the comfort zone as a function of room temperature and relative humidity since this last parameter influences the human thermal sensation and modifies the room temperature perception. The Givoni bioclimatic chart is the result of this process (Figure 1) [47].

Table 1. Status and value of parameters intervening on thermal comfort evaluation.

Parameter	Status/Value
Metabolic level	1 for moderate activity, 3 for intermediate, and 5 for intense
Ambient pressure	~101.3 kPa
Convection coefficient	Calculated from body and ambient temperature or wind speed
Room's wind speed	Measured with an anemometer
Body temperature	~37.0ºC
Clothing factor	0 for nudity, 0.6, 2.4, and 4 for light, medium, and heavy clothing
Ambient temperature	Measured with temperature sensor
Wet body surface	0 for light or null activity, 0.5 for moderate, and 1 for intense
MRT	Calculated from the black globe conditions (Eq. (7))
Energy efficiency	~0.25
Black globe temperature	Determined with internal temperature sensor

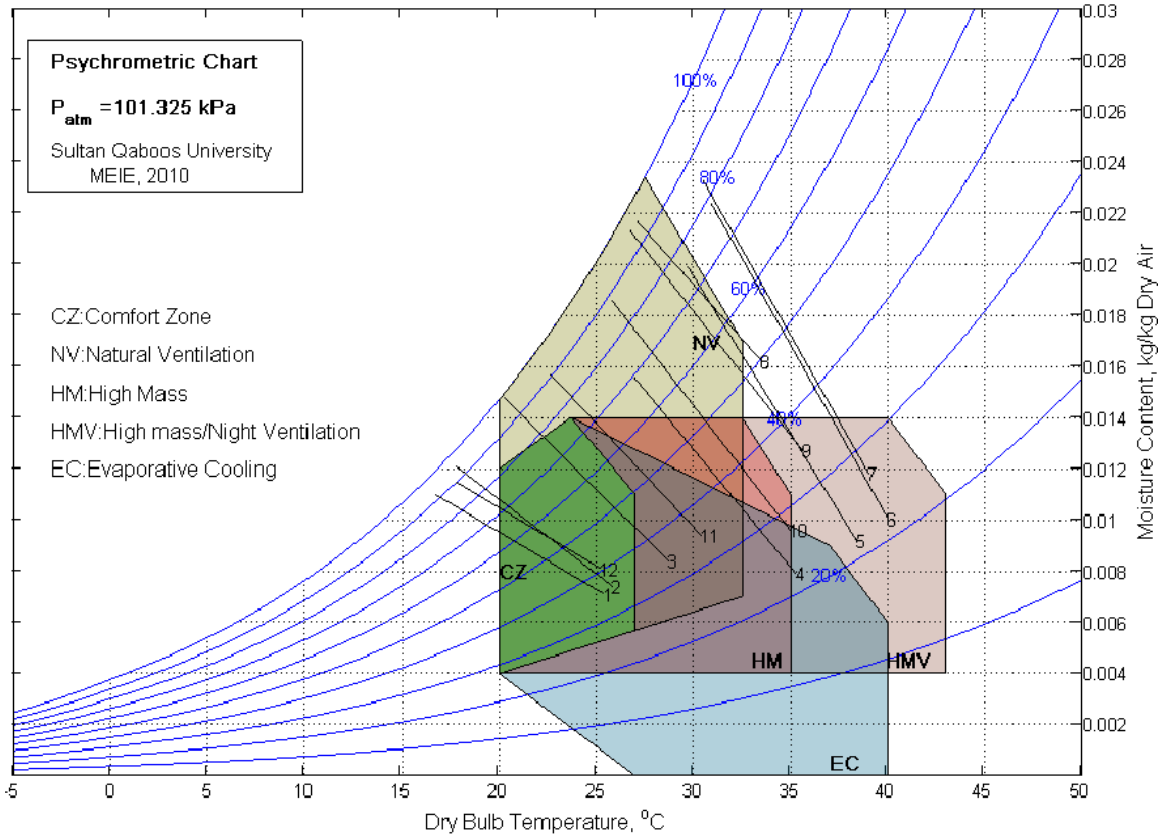

Figure 1. Bioclimatic chart.

The bioclimatic chart, however, does not maintain the comfort conditions if environmental conditions change, such as the monthly mean wind speed, the humidity, and the average temperature. Other factors affecting the comfort zone setting up are clothing changes during people's stay in the room or physical activity variation.

CONTROL SYSTEM

Building air conditioning requires a control system to adapt variable working conditions to the comfort requirements, maximizing energy efficiency. The control system implementation benefits the room air conditioning performance, allowing changes to adapt the operational protocol to variable conditions. The proposed control system is based on the feedback methodology modifying the working conditions of the air conditioning system as a function of the output signal.

The control system portfolio for building air conditioning includes the proportional-integral control unit (PI), differential of proportional-integral (PID), fuzzy logic, neuronal network, and ARMA models. We select the PID methodology because of its high adaptive capacity and easy management.

The PID controller family uses three different actions: proportional (P), integral (I), and derivative (D), which we may use individually or in a combined way. Any possible selection operates identically; given a reference value (set point) for the selected parameter, the PID routine compares it with the measured value, applying an approach method until the differential is below a specific level.

In the PID method, the three combined actions apply to the approaching protocol according to the next expression:

$$u(T) = K_p e(T) + \frac{K_p}{t_i}\int_o^T e(\tau)d\tau + K_p t_d \frac{d}{dt}e(T) \tag{10}$$

K_p is the proportional gain, t_d is a derivative time constant, t_i is the integral time constant, and $e(t)$ is the error function, defined as:

$$e(t) = T_{set} - T_a \tag{11}$$

The function $u(T)$ corresponds to the control action that activates a controller modifying the selected parameter. The PID protocol iterates the process until the comfort conditions in the Fanger equation are fulfilled. First term in Eq. (10) corresponds to the proportional fraction, with the second and third terms accounting for integral and derivative.

Figure 2 shows the PID process flowchart. The term $y(t)$ represents the variable current value, the room temperature in our case.

Applying the PID protocol, the room temperature evolves from the initial to the setup value, *Tset*, being the reference point. Because the comfort zone covers a temperature range, the setup value for the PID protocol corresponds to $Tset+\Delta T$, where ΔT is the temperature interval around the center point temperature of the comfort zone.

The temperature evolution from the initial to the final state depends on the proportional constant, K_p, as shown in Figure 3.

Theoretically, the number of temperature evolution curves is infinite; however, in practice, the number is limited due to the sensor temperature accuracy, which allows only finite temperature variation.

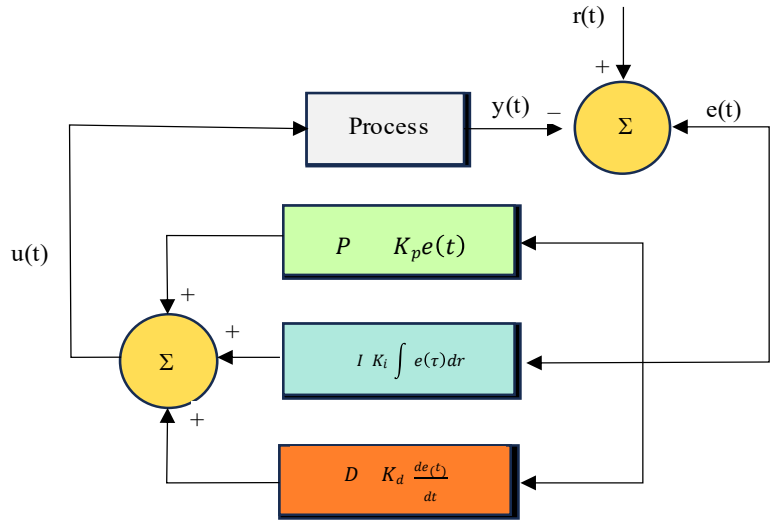

Figure 2. PID process flowchart.

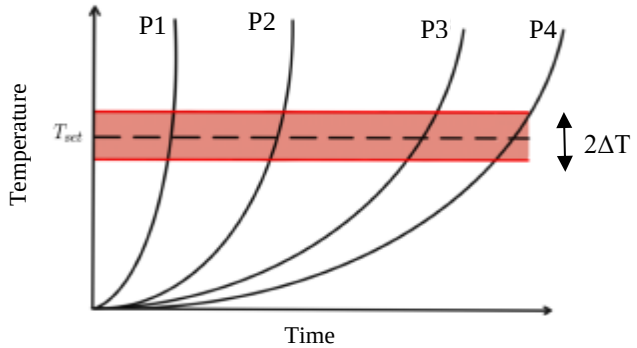

Figure 3. Temperature evolution with time for variable proportional constant.

The temperature interval, 2ΔT, influences the PID process since it defines the temperature range for the comfort zone (Figure 4); if the setup temperature exceeds the comfort zone limits, the process is invalid and requires a new iteration. Therefore, the temperature operates within an error band (Figure 5).

We notice that the comfort zone corresponds to the preset temperature band plus the error band; therefore, the PID protocol should consider this configuration when presetting the temperature for the comfort zone.

Since the temperature evolution curve depends on the available heating time, P1 is the best for a short time, while P4 is the best for a long time. Applying the basic calorimetric equation:

$$\dot{Q} = m_{air} c_{air} \frac{\Delta T_{air}}{\Delta t} = \rho_{air} V_{air} c_{air} \frac{\Delta T_{air}}{\Delta t} \tag{12}$$

We notice that the heating rate, $\Delta T_{air}/\Delta t$, depends on the heating required energy and room size.

PID PROTOCOL AND PID CONTROLLER OPERATION

According to Eq. (10), the PID protocol may use one or more actions depending on operational conditions. The proportional action (P) provides an adjustable output signal, K_p, proportional to the error function. The P-action is immediate and does not consider the temperature inertial trend, causing an offset error. The P-action shows the advantage of approaching the current temperature to the setup value as fast as established by the K_p value; the higher the K_p coefficient, the shorter the approaching time. Nevertheless, it generates an unstable situation with temperature fluctuation around the setup value.

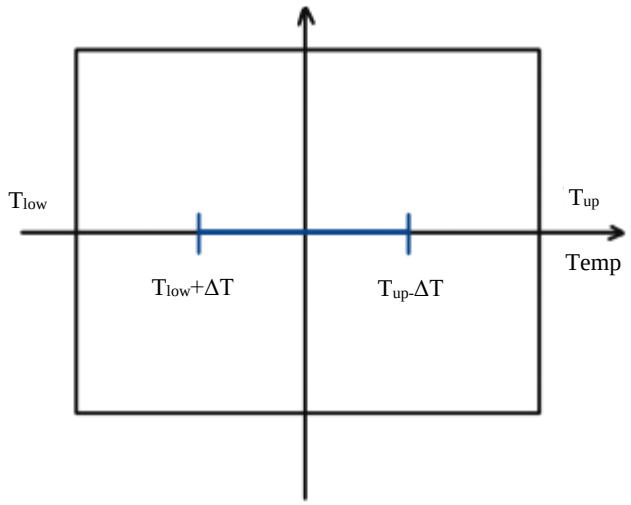

Figure 4. Schematic representation of the comfort zone.

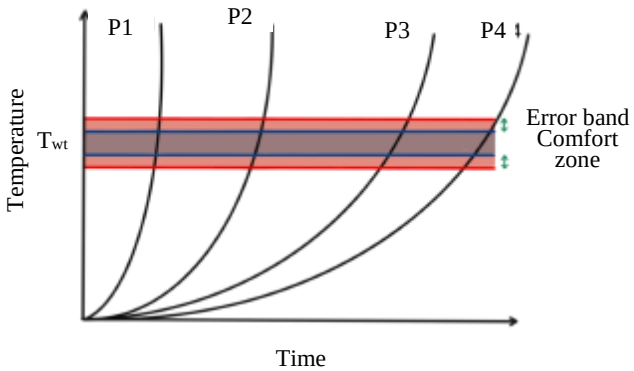

Figure 5. Temperature evolution with time for variable proportional constant including error bands.

The integral action (I) provides an output signal proportional to the cumulative error, slowing down the process as the variable, the building temperature, approaches the setup value. This configuration shows the advantage of accelerating or slowing the room heating process. If we combine the proportional and integral actions (PI), the system reacts to the error value, heating or refrigerating the building as the error is positive or negative.

Combining proportional and derivative actions (PD), we modify the heating rate, increasing or decreasing the heat flow to the building to the most suitable rate, predicting the temperature value at the next step, and improving the process efficiency. However, PD action amplifies the signal noise and generates saturation in the PID controller.

The proportional-integral-derivative action (PID) minimizes the drawbacks of every single action and enhances the advantages, reducing or eliminating instability, minimizing heating time, and improving efficiency.

Initially, the control system collects the setup temperature (T_{set}) and the temperature evolution function (P_j). Since the heating process is not instantaneous, the PID protocol activates the derivate term to ensure the heating process evolves in the right direction, approaching the setup comfort temperature. To this goal, the control system collects the room temperature at regular intervals and determines the heating process direction using the derivative term of the PID protocol.

The PID protocol looks for the maximum efficiency possible and the minimum heating time; therefore, the proportional coefficient, *Kp*, gradually reduces as the room temperature approaches the setup value to avoid overpassing. On the other hand, the integral term adjusts when approaching the setup value to reduce heating flow, increasing the accuracy. The procedure is so because the system operates dynamically, adjusting values according to the error function as the heating process evolves.

OPERATIONAL MODE

The control system regulates the building air conditioning system consisting of an aerothermal unit and wall-mounted radiators (Figure 6). The aerothermal unit operates under a Rankine thermodynamic cycle, heating water in a primary circuit for house heating and a secondary circuit for household inhabitant's hygiene. The aerothermal unit heats the water of the primary circuit between the heating tank and the aerothermal unit until reaching the setup temperature. The heating tank heats sanitary water in the hot water tank when needed through a close circuit between tanks (secondary circuit); water circulates using a pump.

The control unit prioritizes sanitary hot water over household heating or refrigerating; if the hot water tank reduces its temperature, the control unit derives the hot water generation from the heating to the hot water tank until achieving setup temperature for sanitary use. Since the sanitary water demand is unpredictable, the control unit applies a high proportional coefficient to accelerate hot water tank thermal loading. Because the network water supply is always at a lower temperature than required for household sanitary services, the derivative term does not apply, and the PID protocol reduces to proportional and integral terms (PI action).

At the building heating process the control unit applies the PID protocol to reduce heating time, maximize heat transfer, and optimize energy efficiency. During this process, the control unit evaluates the heat demand applying the Fanger equation and collecting data from sensors and database to determine the energy requirements and establish the proportional coefficient, K_p. Because the black globe is not a part of the building furniture or household appliances, the mean radiant temperature is unknown; therefore, the control unit estimates the MRT value, considering an initial value equal to the room temperature and iterating until the Fanger equation fulfills, provided the values of all the other parameters are known.

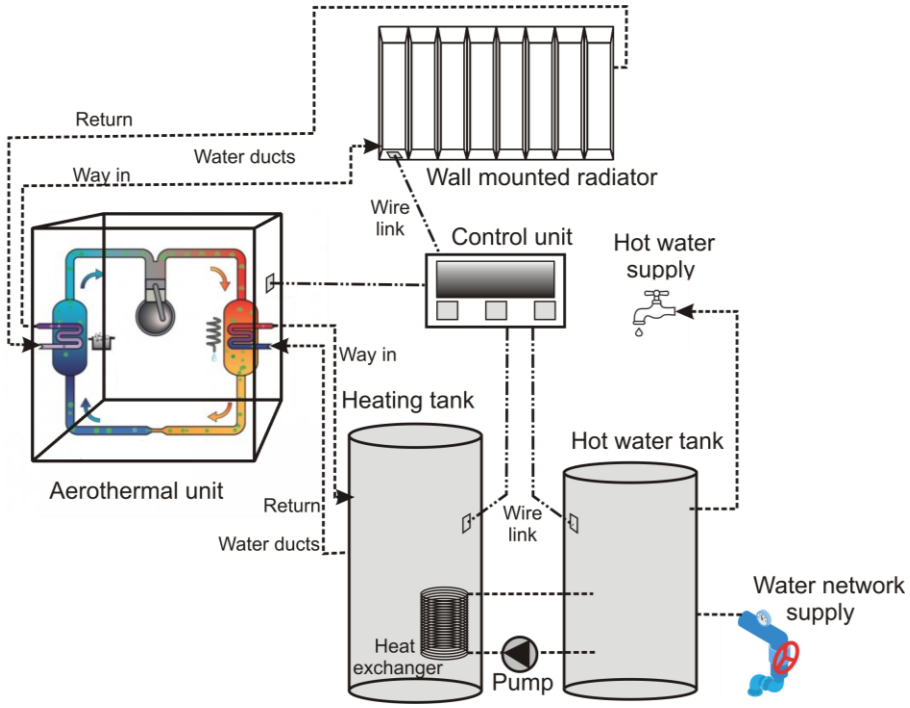

Figure 6. Layout of the household installation.

Once the MRT is estimated, the control unit applies the PID protocol to heat the building using the average value for the variable parameters, metabolic level, clothing factor, and wind speed. The control unit applies the default heating curve recommended by the aerothermal unit manufacturer for the operating climatic zone, and calculates the function error at the first PID protocol step; if the error function exceeds a setup value, the PID protocol modifies the K_p coefficient and recalculates the *u(T)* function. The process develops at short integral time to avoid deviation from the expected trend.

NUMERICAL SIMULATION

Applying data for standard conditions (Table 2), and considering a metabolic level variation from 1 to 5 in 0.25 steps, we obtain the comfort temperature for every human activity condition (Figure 7).

Table 2. Simulation conditions.

ADU (m^2)	η	P_a (kPa)	T_a (°C)	f_{cl}	T_{MRT} (°C)	v (m/s)
0.30	0.85	101.3	16.0	0.5	25.0	0.25

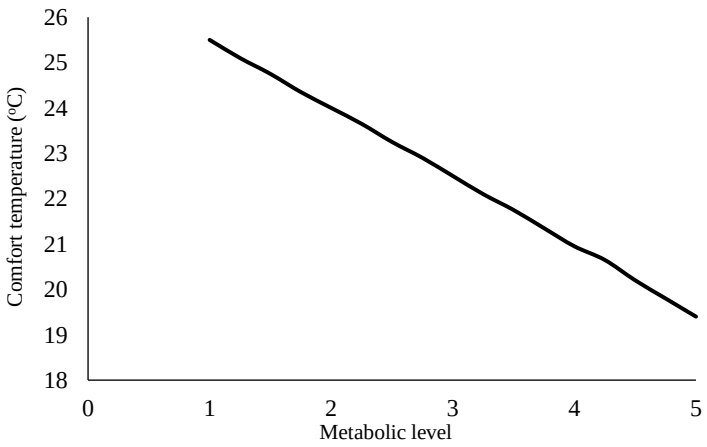

Figure 7. Comfort temperature evolution with metabolic level.

We consider a standard human body for the ADU value and metabolic to heat energy conversion efficiency. The operating pressure is the standard value. The ambient temperature is the average over a wide range of climatic zones. The Mean Radiant Temperature corresponds to the average value of many variable room thermal conditions. The clothing factor corresponds to the average value of conventional dressing for current human activities. Finally, wind speed considers the inside room air movement due to ventilation.

We notice that the comfort temperature inversely depends on the metabolic level. The correlation between the two parameters shows the following mathematical relation:

$$T_{comfort} = -1.5157M + 27.029 \quad \left(R^2 = 0.9998\right) \tag{13}$$

The simulation results are coherent with expected people's thermal sensations since the room temperature to achieve a neutral thermal condition decreases as people increase their physical activity and metabolic level. If we average over the whole metabolic range, the comfort temperature is 22.5ºC, exceeding by 1.5ºC the standard value for the comfort conditions according to bioclimatic studies and analysis [48]. Nevertheless, the standard comfort temperature accepted by the World Health Organization (WHO) [48] corresponds to a medium metabolic level, for which our simulation produces an average comfort temperature of 20.95ºC, only 0.05ºC below the standard value of 21ºC.

Table 3 shows the comparative analysis between comfort temperature standard values and simulation results for various metabolic level ranges.

Table 3. Comparative analysis between comfort temperature standard values and simulation results for various metabolic level ranges.

Metabolic level range		**Low**	**Medium**	**High**
Temperature (ºC)	Standard	24.0	21.0	18.0
	Simulation	24.2	20.95	19.4
Deviation (%)		0.83	0.02	7.22

We notice that the simulation predicts highly accurate comfort temperature values for the low and medium metabolic levels but slightly deviates for high physical activity.

ENERGY BALANCE

Because human activity may vary during the day, the metabolic level and the comfort temperature do as well; therefore, it is necessary to adapt the heating process to the thermal requirements. To this goal, the control unit evaluates the body heat generation from the people's skin infrared emission since the metabolic level directly relates to the body heat generation through a specific factor. The determination of the correlation factor derives from the basal temperature analysis (Eq. (3)).

The heat generation and basal temperature correlate through a linear dependence as in the following expression:

$$T_s = -0.1067H + 35.7 \quad \left(R^2 = 0.9999\right) \tag{14}$$

Or

$$T_s = -0.1067 f_H M + 35.7 \quad \left(R^2 = 0.9999\right) \tag{15}$$

f_H is the correlation factor between H and M.

Applying Eq. (15) to variable metabolic level, and considering the basal temperature evolves from a maximum of 35.2ºC to a minimum of 33.0ºC, we obtain f_H=5.0; therefore, we can represent the body skin temperature evolution with metabolic level as:

$$T_{skin} = 0.5335M + 27.7 \quad \left(R^2 = 1\right) \tag{16}$$

Eq. (16) predicts a body skin temperature between 32.7 and 34.8ºC, with an average value of 33.8ºC, in close agreement with a precedent study [49], showing a deviation lower than 0.1ºC.

The heating process adaptation requires a continuous body's thermal activity (heat generation) evaluation and the change in heat flow from the power unit to the building. Since the heat flow injection modifies the building temperature, the control system should actuate over the heat power generation by controlling the flow rate of the heat carrier fluid and the operational temperature [50].

Based on the basic calorimetric equation, the heat flow injection is:

$$\dot{Q} = F_R \dot{q} \tag{17}$$

Where $\dot{q}$ represents the heat transfer fluid calorific value, and F_R is the heat transfer coefficient.

Depending on the heating system, $\dot{Q}$ comes differently. Because wall mounted radiators, radiant floors, or forced hot air circulation are the current heating systems today, Eq. (17) adopts different forms.

Forced Hot Air Circulation

The system uses a fan-coil to extract energy from circulating water in a secondary circuit, heating the air blown by a fan inserted in a ceiling duct. The hot air is injected into the room, raising the temperature. Figure 8 shows a schematic representation of the heat exchange system.

The heat flow to achieve the comfortable temperature is given by:

$$\dot{Q} = m_a c_a \frac{\Delta T_r}{\Delta t} \tag{18}$$

$\dot{m}_a$ and c_a are the mass flow and specific heat of injected air, ΔT_r is the room temperature increase, and Δt is the heating time until reaching the comfort temperature.

Since the fan-coil supplies the energy:

$$\dot{m}_a c_a \frac{\Delta T_r}{\Delta t} = F_{R,f-c} \dot{m}_w c_w \frac{\Delta T_w}{\Delta t} \rightarrow \Delta T_r = F_{R,f-c} \frac{\dot{m}_w c_w}{\dot{m}_a c_a} \Delta T_w = F_{R,f-c} \frac{\dot{m}_w c_w}{\dot{m}_a c_a} \left(T_{PID} - T_{w(return)}\right) \tag{19}$$

The subscript *w* accounts for the water circulating throughout the coil.

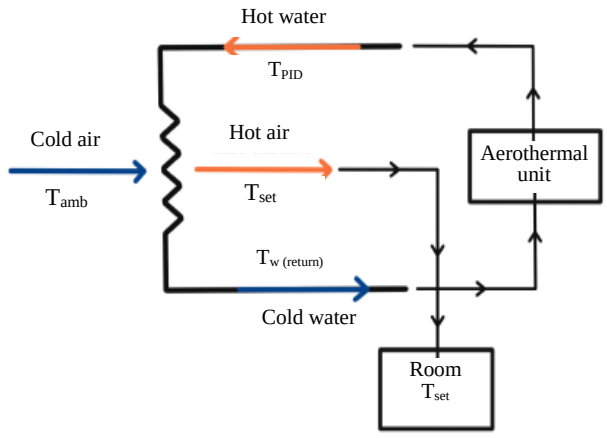

Figure 8. Schematic view of the fan-coil heating system.

Analyzing Eq. (19), we observe that the room temperature increase depends on water and air mass flows and the temperature difference between the setup value at the control system and water return.

Once the control system sets up the PID value, the temperature difference remains constant, and the only variable parameter is the air mass flow because the water mass flow is also constant; therefore, the control system can modify the heating process by increasing or lowering the air mass flow. Rearranging Eq. (19):

$$\Delta T_r = \frac{C_1^{f-c}}{\dot{m}_a} \tag{20}$$

With

$$C_1^{f-c} = F_{R,f-c}\frac{\dot{m}_w c_w}{c_a}\left(T_{PID} - T_{w(return)}\right) \tag{21}$$

On the other hand, by applying a reverse thermal process, we can determine the PID temperature through the expression:

$$T_{PID} = \frac{\dot{m}_a c_a}{\dot{m}_w c_w}\frac{\Delta T_r}{F_{R,f-c}} + T_{w(return)} \tag{22}$$

There is a linear dependence between the PID and room temperature provided all parameters are set up, except the room temperature, as in:

$$T_{PID} = \Delta T_r\left(\frac{\dot{m}_a c_a}{F_{R,f-c}\dot{m}_w c_w} + T_{w(return)}\right) = C_2^{f-c}\Delta T_r \tag{23}$$

With

$$C_2^{f-c} = \left(\frac{\dot{m}_a c_a}{F_{R,f-c}\dot{m}_w c_w} + T_{w(return)}\right) \tag{24}$$

The control system can adjust the PID temperature to increase room temperature by modifying the air and water mass flow values since the linear dependence constant changes.

Wall Mounted Radiators

Wall mounted radiators emit thermal energy based on the temperature difference between the radiator and the room. Applying the Stefan-Boltzmann law:

$$\dot{Q} = F_{R,rad}\sigma\varepsilon S_{rad}\left(T_{rad}^4 - T_r^4\right) \tag{25}$$

Considering current operational temperatures for the wall radiator and room, the following relation applies:

$$T_{rad}^4 = f_T T_r^4 \rightarrow T_r^4 = \frac{T_{rad}^4}{f_T} \tag{26}$$

With a minimum of 95% accuracy.

The factor f_T correlates to wall radiator temperature as in:

$$f_T = \left(0.0005T_{rad}^2 - 0.0255T_{rad} + 1.5275\right) \quad (R^2 = 0.9966) \tag{27}$$

Combining Eqs. (25) and (26):

$$\dot{Q} = F_{R,rad}\sigma\varepsilon S_{rad}T_{rad}^4\left(1 - \frac{1}{f_T}\right) \tag{28}$$

Considering a linear water temperature decrease inside the wall radiator:

$$T_{rad} = \frac{T_{PID} + T_{w(return)}}{2} = \frac{T_{PID} + T_r + 2}{2} \tag{29}$$

Since the temperature difference between the water return and the room is around 2ºC.
Replacing Eq. (29) in Eq. (28), and combining with Eq. (18):

$$m_a c_a \Delta T_r = F_{R,rad}\sigma\varepsilon S_{rad}\left(\frac{T_{PID} + T_r + 2}{2}\right)^4\left(1 - \frac{1}{f_T}\right) \tag{30}$$

Clearing in Eq. (30):

$$\Delta T_r = F_{R,rad}\sigma\varepsilon S_{rad}\left(\frac{T_{PID} + T_r + 2}{2}\right)^4\left(1 - \frac{1}{f_T}\right)\frac{1}{m_a c_a} \tag{31}$$

And

$$T_{PID} = 2\left[\frac{m_a c_a}{F_{R,rad}\sigma\varepsilon S_{rad}}\left(\frac{f_T}{f_T - 1}\right)\Delta T_r\right]^{1/4} - \left(T_r + 2\right) \tag{32}$$

The control system regulates the PID temperature by modifying the wall radiator temperature, on which the factor f_T depends.

Radiant Floor

The radiant floor exchanges heat with the room through a water coil incrusted in the soil. The thermal energy exchange responds to the equation:

$$\dot{Q} = F_{R,rf}h_c S_{rf}\left(T_{rad} - T_r\right) \tag{33}$$

S_{rf} is the radiant floor surface, and h_c is the convection coefficient.
Combining Eqs. (18), (29) and (33):

$$m_a c_a \Delta T_r = F_{R,rf}h_c S_{rf}\left(\frac{T_{PID} - T_r + 2}{2}\right) \tag{34}$$

From which, we have:

$$T_{PID} = \frac{2m_a c_a}{F_{R,rf}h_c S_{rf}}\left(\frac{T_r}{2} + 1\right)\Delta T_r \tag{35}$$

Eq. (35) shows that the control system regulates the PID temperature according to the room temperature.

We may combine radiation and convection to heat the building quicker or use a single mechanism if the energy requirements are not very exigent.

CONTROL SYSTEM

Heat power generation comes from the aerothermal unit, which transfers energy from the refrigerant fluid to water at a primary circuit between the aerothermal unit and the heating tank. Primary circuit water temperature depends on the selected working curve and ambient temperature, as shown in Figure 9; we notice that for an ambient temperature of –15ºC and selected heating curve of 0.4, the primary circuit water temperature is 40ºC.

If the ambient temperature remains constant, and heating flow needs to increase or reduce because of building higher or lower energy demand, what happens when people's activity and metabolic level increase or diminish; the control system should move the heating curve to a higher or lower value. For instance, if the primary circuit required water temperature is 60ºC due to higher energy demand because of lower human activity, the heating curve needs to move from 0.4 to 1.0 (continuous red line); if the required water temperature is 30ºC because the human activity reduces, the heating curve is 0.2 (dashed red line).

If the ambient temperature increases and the energy demand increases too, the water temperature should rise. We observe that for ambient temperature rise from –15 to 0ºC, and water temperature increase to 50ºC (continuous blue line), the heating curve is 1.2; on the contrary, if water temperature needs to be lower, for instance, 25ºC, the heating curve is now 0.1 (dashed blue line).

EXPERIMENTAL TESTS

Retrieving data from Figure 7 and applying it to specific building conditions (Table 4), we run experimental tests to determine the energy requirements to maintain the comfort state.

K represents the global thermal loss coefficient for the building envelope, and S_L is the envelope surface. The volume corresponds to the inner space.

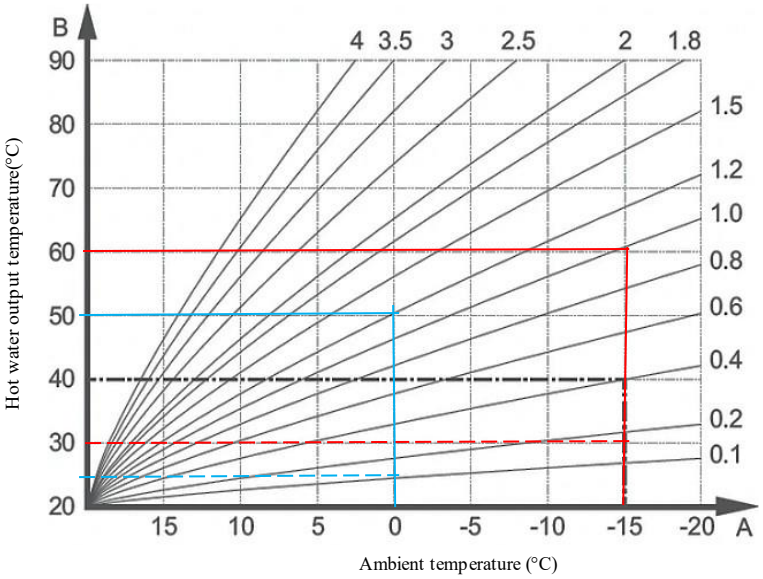

Figure 9. Heating curves for the aerothermal unit.

Table 4. Building characteristics.

Parameter	Volume (m^3)	K ($W/m^2 \cdot K$)	S_L (m^2)
Value	157.5	0.53	96

The operating conditions for the tests are (Table 5). The surface correction factor corresponds to the ratio of effective to cross-section surface. Although some parameters like ambient temperature, air density, and specific heat are not strictly constant, they suffer from low variation; thus, we consider them constant. The loop time for the running tests is 10 min.

Table 5. Operating conditions and system characteristics for test running.

Parameters	Values
Air density (kg/m^3)	1.022
Air specific heat (kJ/kg·ºC)	1.066
Room initial temperature (ºC)	18
Room set up temperature (ºC)	22
Fan coil output temperature (ºC)	27
Aerothermal unit water mass flow (kg/min)	45
Ambient temperature (winter) (ºC)	5
Ambient temperature (spring/autumn) (ºC)	15
Network water temperature (winter) (ºC)	8
Network water temperature (spring/autumn) (ºC)	12
Water density (kg/m^3)	998
Radiant surface (m^2)	3.256
Radiant surface emissivity	0.9
Heat transfer factor (fan coil)	0.98
Heat transfer factor (heat exchanger)	0.92
Surface correction factor (convection)	4
Surface correction factor (convection + radiation)	1.1

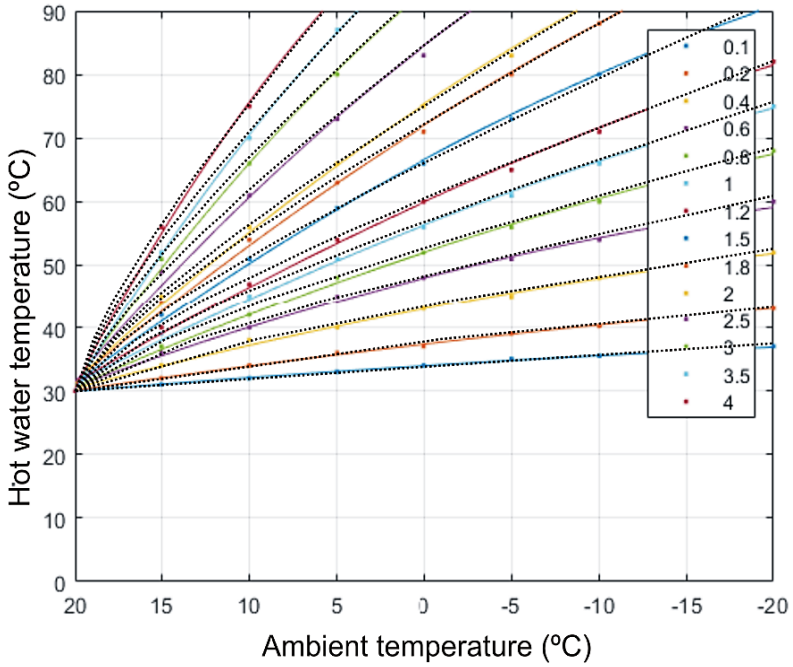

Figure 10. Correlation between theoretical and manufacturer heating curves for the aerothermal power unit.

Before starting the tests, we apply the developed algorithms to reproduce the heating curves using the specific parameter values and operational conditions. Figure 10 shows the simulation results and the aerothermal unit heating curves provided by the manufacturer. Dashed lines correspond to

manufacturer heating curves, while colored lines represent the simulated ones. Table 6 shows the correlation coefficient between manufacturer and simulated heating curves for every case.

Table 6. Correlation coefficient for manufacturer and simulated heating curves.

Curve	**0.1**	**0.2**	**0.4**	**0.6**	**0.8**	**1.0**	**1.2**
R^2	0.9969	0.9979	0.9971	0.9961	0.9985	0.9983	0.9981
Curve	1.5	1.8	2.0	2.5	3.	3.5	4.0
R^2	0.9989	0.9987	0.9980	09971	0.9982	0.9998	0.9993

We observe the good correlation between simulated and manufacturer heating curves, proving the validity of the proposed algorithms.

Figures 11 and 12 show the predicted and experimental values for 120 min room thermal conditioning time.

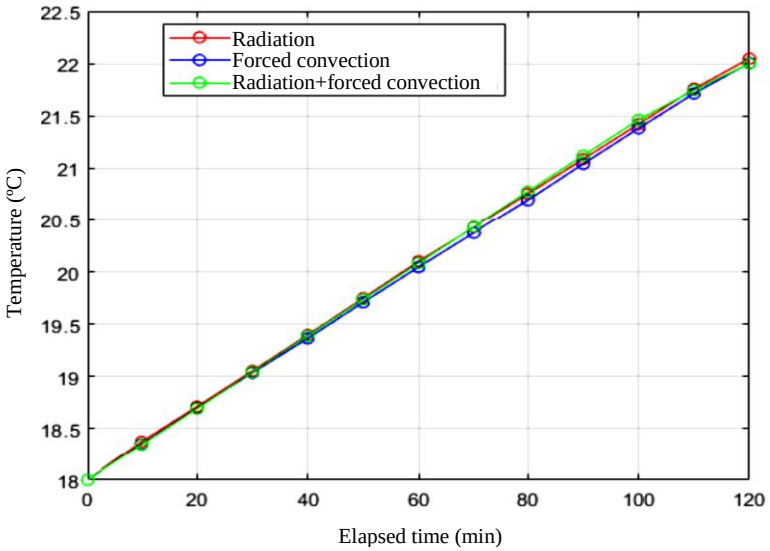

Figure 11. Predicted (colored lines) and experimental values (round circles) of comfort temperatures for spring and autumn. Air conditioning time: 120 min.

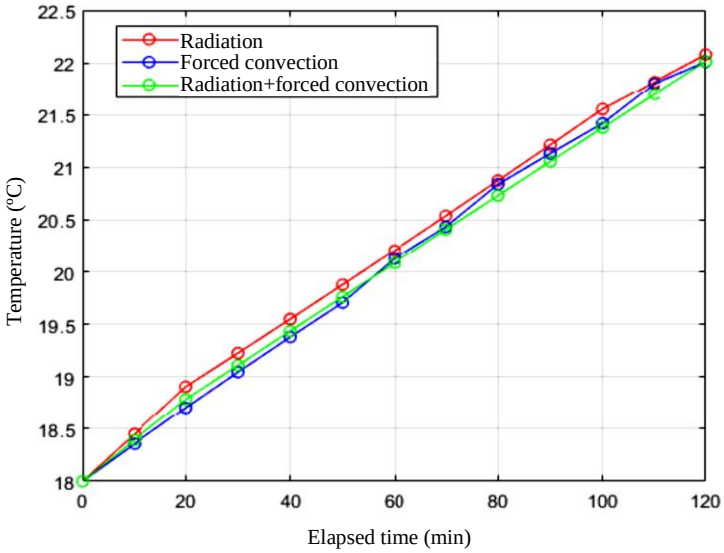

Figure 12. Predicted (colored lines) and experimental values (round circles) of comfort temperatures for winter. Air conditioning time: 120 min.

We notice the excellent correlation between predicted values and experimental data, a consequence of the high accuracy in the developed algorithms for predicting room thermal behavior using the PID technique applied to the control system that regulates the heating curve for optimum performance.

Repeating the process for room thermal conditioning time of 90, 60 and 30 min, we obtain (Figures 13–18):

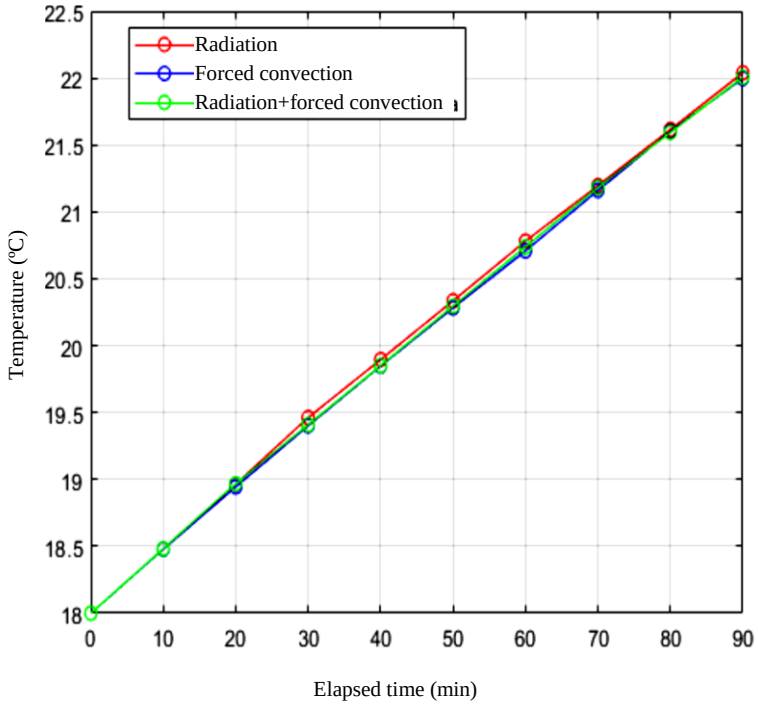

Figure 13. Predicted (colored lines) and experimental values (round circles) of comfort temperatures for spring and autumn. Air conditioning time: 90 min.

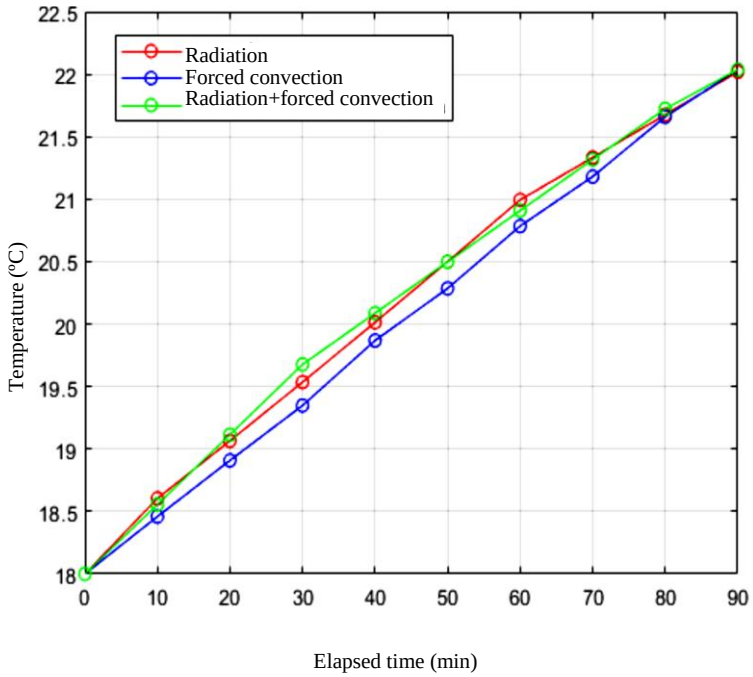

Figure 14. Predicted (colored lines) and experimental values (round circles) of comfort temperatures for winter. Air conditioning time: 90 min.

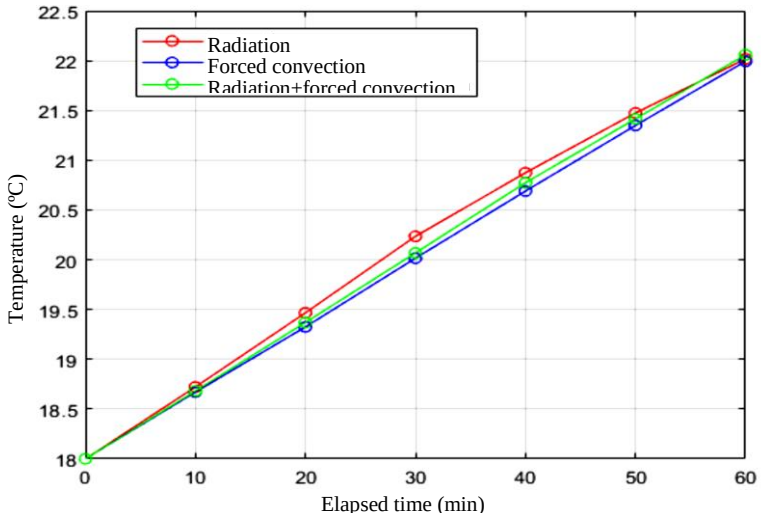

Figure 15. Predicted (colored lines) and experimental values (round circles) of comfort temperatures for spring and autumn. Air conditioning time: 60 min.

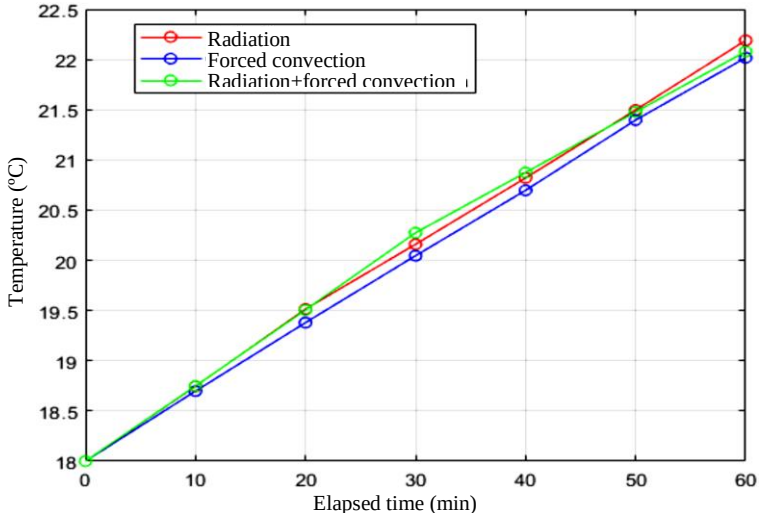

Figure 16. Predicted (colored lines) and experimental values (round circles) of comfort temperatures for winter. Air conditioning time: 60 min.

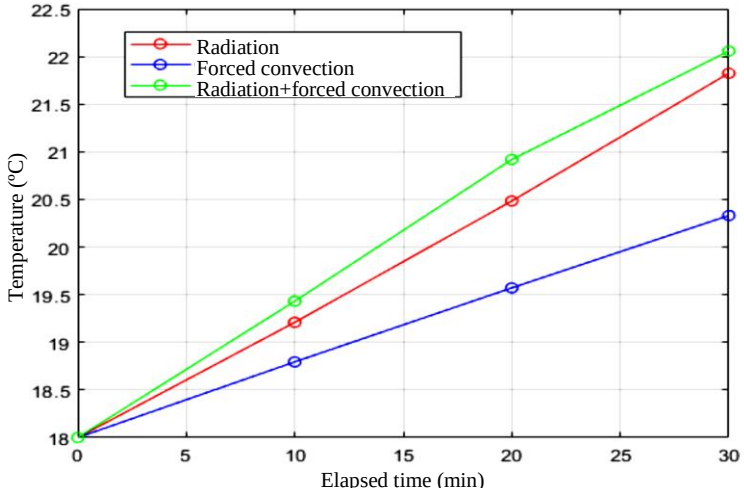

Figure 17. Predicted (colored lines) and experimental values (round circles) of comfort temperatures for spring and autumn. Air conditioning time: 30 min.

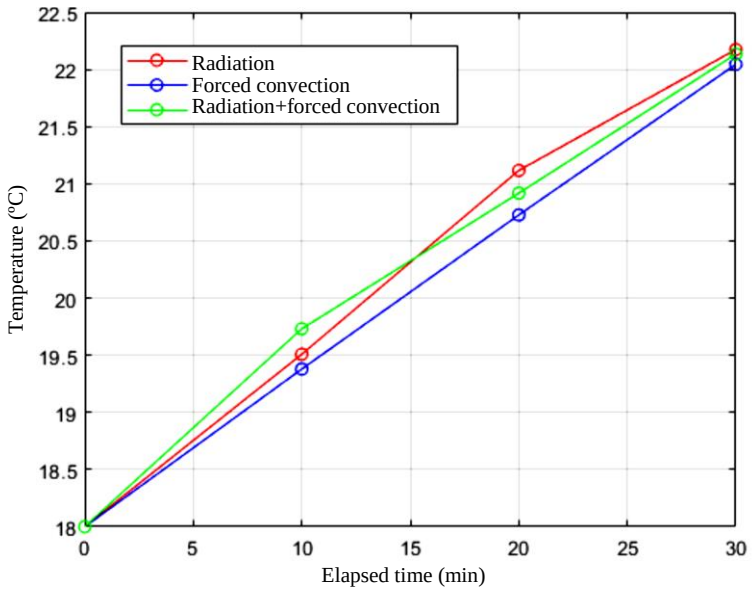

Figure 18. Predicted (colored lines) and experimental values (round circles) of comfort temperatures for winter. Air conditioning time: 30 min.

CONCLUSION

We develop a theoretical method for building air conditioning based on comfort conditions by fulfilling the Fanger equation, considering environmental parameters (ambient temperature), metabolic rate, and people's physical activity (internal heat generation). Theoretical predictions of building temperature match experimental tests run in an inhabited house with accuracy higher than 99%.

The prediction of building thermal behavior is based on a control system assisted by the PID technique applied to an aerothermal unit that powers the building heating system. The aerothermal unit operates with variable heating curves related to the heating power level, which regulates the water temperature used for heating the building. The control system selects the heating curve based on building thermal energy requirements.

We use three methods for heating the building: radiation, forced convection, and radiation-forced convection hybrid method. The combined one provides the best results with higher efficiency among the three methods.

The radiation plus forced convection method reduces energy use due to a lower heating curve level (lower heating power), improving efficiency and requiring less power from the energy source. Besides, it reduces the heating time to reach the setup temperature inside the building.

Experimental tests run for the building thermal conditioning time of 30, 60, 90, and 120 min show a close agreement with predicted thermal behavior, with a correlation coefficient near 100%.

REFERENCES

1. Che WW, Tso CY, Sun L, Ip DY, Lee H, Chao CY, Lau AK. Energy consumption, indoor thermal comfort and air quality in a commercial office with retrofitted heat, ventilation and air conditioning (HVAC) system. Energy Build. 2019; 201: 202–215.
2. Pérez-Lombard L, Ortiz J, Pout C. A review on buildings energy consumption information. Energy Build. 2008; 40(3): 394–398.
3. Korolija I. Heating, ventilating and air-conditioning system energy demand coupling with building loads for office buildings. Doctoral Thesis. England: De Montfort University; 2011.
4. Kreider JF. Handbook of heating, ventilation, and air conditioning. CRC press; United States. 2000.

5. Berardi U. Building energy consumption in US, EU, and BRIC countries. Procedia Eng. 2015; 118: 128–136.
6. Yang L, Yan H, Lam JC. Thermal comfort and building energy consumption implications–a review. Appl Energy. 2014; 115: 164–173.
7. Zhou Y, Eom J, Clarke L. The effect of global climate change, population distribution, and climate mitigation on building energy use in the US and China. Clim Change. 2013; 119: 979–992.
8. Rastogi P. On the sensitivity of buildings to climate: the interaction of weather and building envelopes in determining future building energy consumption. Doctoral Thesis. (No. 6881). Switzerland: EPFL; 2016.
9. Li DH, Yang L, Lam JC. Impact of climate change on energy use in the built environment in different climate zones–a review. Energy. 2012; 42(1): 103–112.
10. Zhao HX, Magoulès F. A review on the prediction of building energy consumption. Renew Sustain Energy Rev. 2012; 16(6): 3586–3592.
11. Fonseca JA, Nevat I, Peters GW. Quantifying the uncertain effects of climate change on building energy consumption across the United States. Appl Energy. 2020; 277: 115556.
12. Nicol F, Humphreys M, Roaf S. Adaptive thermal comfort: principles and practice. Routledge; U.K. 2012.
13. Karmakar G, Kabra A, Ramamritham K. Maintaining thermal comfort in buildings: feasibility, algorithms, implementation, evaluation. Real-Time Syst. 2015; 51: 485–525.
14. Sansaniwal SK, Mathur J, Mathur S. Review of practices for human thermal comfort in buildings: present and future perspectives. Int J Ambient Energy. 2022; 43(1): 2097–2123.
15. De Dear RJ, Brager GS. Thermal comfort in naturally ventilated buildings: revisions to ASHRAE Standard 55. Energy Build. 2002; 34(6): 549–561.
16. Mui KW, Tsang TW, Wong LT. Bayesian updates for indoor thermal comfort models. J Build Eng. 2020; 29: 101117.
17. De Dear R, Schiller Brager G. The adaptive model of thermal comfort and energy conservation in the built environment. Int J Biometeorol. 2001; 45: 100–108.
18. OECD (Organisation for Economic Co-operation and Development). [Online]. https://www.oecd.org/en.html
19. McNeil MA, Letschert VE. Future air conditioning energy consumption in developing countries and what can be done about it: the potential of efficiency in the residential sector. Berkeley, California: Lawrence Berkeley National Laboratory; 2008.
20. Berardi U. A cross-country comparison of the building energy consumptions and their trends. Resour Conserv Recy. 2017; 123: 230–241.
21. IRENA. Power to heat and cooling: Status. [Online]. IRENA (International Renewable Energy Agency). https://www.irena.org/Innovation-landscape-for-smart-electrification/Power-to-heat-and-cooling/Status [Accessed online: 11/11/2024]
22. Santamouris M, Vasilakopoulou K. Present and future energy consumption of buildings: Challenges and opportunities towards decarbonisation. e-Prime-Advances in Electrical Engineering, Electronics and Energy. 2021; 1: 100002.
23. Standard 55-Thermal Environmental Conditions for Human Occupancy. ANSI/ASHRAE Standard 55. 2023 Edn. USA: ASHRAE. Shaping Tomorrow's Built Environment Today. 2023.
24. Sala M, Gallo C, Sayigh AAM, editors. Architecture-Comfort and Energy. Elsevier; Netherlands. 1999.
25. Fanger PO. The new comfort equation for indoor air quality. ASHRAE (American Society of Heating, Refrigeration and Air-Conditioning Engineers) Journal; (USA). 1989; 31: 10.
26. Humphreys MA, Hancock M. Do people like to feel 'neutral'? Exploring the variation of the desired thermal sensation on the ASHRAE scale. Energy Build. 2007; 39(7): 867–874.
27. MacPherson RK. Studies in the preferred thermal environment. Archit Sci Rev. 1963; 6(4): 183–189.
28. Givoni B. Climate considerations in building and urban design. John Wiley & Sons; United States. 1998.

29. Hutchison JS, Ward RE, Lacroix J, Hébert PC, Barnes MA, Bohn DJ, et al. Hypothermia therapy after traumatic brain injury in children. N Engl J Med. 2008 Jun; 358(23): 2447–56. doi:10.1056/NEJMoa0706930. PMID 18525042.
30. Pryor JA, Prasad AS. Physiotherapy for Respiratory and Cardiac Problems: Adults and Paediatrics. 4th Edn. Elsevier Health Sciences; 2008. ISBN 978-0702039744.
31. Mateusz Mucha, James Mathison, Dominika Śmiałek. BSA Calculator - Body Surface Area. [Online]. Mni Calculator.
32. Burton R. Estimating body surface area from mass and height: theory and the formula of Du Bois and Du Bois. Ann Hum Biol. 2009 Jul; 35(2): 170–184.
33. Mosteller R. Simplified calculation of body-surface area. N Engl J Med. 1987 Oct; 317(17): 1098.
34. Haycock G, Schwartz G, Wisotsky D. Geometric method for measuring body surface area: a height-weight formula validated in infants, children, and adults. J Pediatr. 1987 Jul; 93(1): 62–6.
35. Gehan E, George S. Estimation of human body surface area from height and weight. Cancer Chemother Rep. 1970 Aug; 54(4): 225–35.
36. Fujimoto S, et al. Studies on the Physical Surface Area of Japanese. Nippon Eiseigaku Zasshi (Japanese Journal of Hygiene). 1968; Dec; 23(5): 443–50.
37. Matzarakis A, Rutz F, Mayer H. Estimation and calculation of the mean radiant temperature within urban structures. In Biometeorology and Urban Climatology at the Turn of the Millenium. de Dear RJ, Kalma JD, Oke TR, Auliciems A, editors. Selected Papers from the Conference ICB-ICUC. 2000; 99: 273–278.
38. Matzarakis A. Estimation and calculation of the mean radiant temperature within urban structures, Manual to Rayman. Germany: University of Freiburg; 2000.
39. Fanger PO. Thermal Comfort: Analysis and Applications in Environmental Engineering. Copenhagen: Danish Technical Press; 1970.
40. Engineers Edge. (2025). Mean Radiant Temperature Formula and Calculator. [online] Engineersedge.com. Available from: https://www.engineersedge.com/calculators/mean_radiant_temperature_15726.htm.
41. Herman IP. Metabolism: Energy, Heat, Work, and Power of the Body. Physics of the Human Body. Cham: Springer; 2007; 319–403.
42. Gnaiger E. Physiological calorimetry: Heat flux, metabolic flux, entropy and power. Thermochim Acta. 1989; 151: 23–34.
43. Luo M, Wang Z, Ke K, Cao B, Zhai Y, Zhou X. Human metabolic rate and thermal comfort in buildings: The problem and challenge. Build Environ. 2018; 131: 44–52.
44. Davis Lawrence. Efficiency of the Human Body. 10.9: Efficiency of the Human Body. [Online]. Physics LibreTexts [Accessed online: 12/11/2024]
45. Eshkorfu OOH, Hanafi ZB. Analyzing elements the climate Hun city an internal comfy house in Libya. In IUKL international postgraduate colloquia (IIPC 2016), infrastructure University Kuala Lumpur. 2016; 423–438.
46. Sayigh A, Marafia AH. Thermal comfort and the development of bioclimatic concept in building design. Renew Sustain Energy Rev. 1998; 2(1–2): 3–24.
47. Szokolay S. Introduction to architectural science. Routledge; U.K. 2012.
48. Givoni B. Comfort, climate analysis and building design guidelines. Energy Build. 1992; 18(1): 11–23.
49. WHO. (2018 Nov 23). WHO Housing and Health Guidelines. [Online]. World Health Organization (WHO). ISBN 978-92-4-155037–6.
50. Barraza-Gómez F, Hecht-Chau G, Báez-San-Martín E, Toro-Salinas A, Henriquez M, García-Pelayo S, Cuevas MJ., Alvear-Ordenes I. Relationship Between Surface Temperature, Body Composition and Anthropometric Indicators of Obesity and Overweight. Int J Morphol. 2023; 41(6).

